The Astronomical Journal, 129:1163–1170, 2005 February

THE THIRD VLBA CALIBRATOR SURVEY: VCS3

L. Petrov
NVI, Inc., 7257D Hanover Parkway, Greenbelt, MD 20770; Leonid.Petrov@lpetrov.net

Y. Y. Kovalev[1]
National Radio Astronomy Observatory, P.O. Box 2, Green Bank, WV 24944; and Astro Space Center, P. N. Lebedev Physical Institute, ulitsa Profsoyuznaya 84/32, 117997 Moscow, Russia;
ykovalev@nrao.edu

E. Fomalont
National Radio Astronomy Observatory, 520 Edgemont Road, Charlottesville, VA 22903-2475;
efomalon@nrao.edu

and

D. Gordon
Raytheon ITSS, Code 926, NASA Goddard Space Flight Center, Greenbelt, MD 20771;
dgg@leo.gsfc.nasa.gov
Received 2004 September 28; accepted 2004 October 20

ABSTRACT

We present the third extension to the Very Long Baseline Array (VLBI) Calibrator Survey, containing 360 new sources not previously observed with very long baseline interferometry (VLBI). The survey, based on three 24 hour VLBA observing sessions, fills the areas on the sky above declination -45° where the calibrator density is less than one source within a 4° radius disk at any given direction. The positions were derived from astrometric analysis of the group delays determined at 2.3 and 8.6 GHz frequency bands using the CALC/SOLVE software package. The VCS3 catalog of source positions, plots of correlated flux density versus length of projected baseline, and contour plots and FITS files of naturally weighted CLEAN images, as well as calibrated visibility function files, are available electronically from the Goddard Geodetic VLBI Group.

Key words: astrometry — catalogs — quasars: general — radio continuum: general — reference systems — techniques: interferometric

Online material: machine-readable table

1. INTRODUCTION

Catalogs of positions of compact radio sources with the highest precision are the basis for many applications. Among these are imaging faint radio sources in phase-referencing mode, monitoring Earth's rotation, space geodesy, and space navigation. The method of VLBI, first proposed by Matveenko et al. (1965), allows one to determine the positions of sources with nanoradian precision (1 nrad $\approx$ 0.2 mas). The first catalog of source positions determined with VLBI (Cohen & Shaffer 1971) contained only 35 sources. It is desirable for the aforementioned applications to have many more sources. In 1998 the ICRF catalog of 667 sources, produced by analyzing VLBI observations made in the framework of space geodesy programs, was published (Ma et al. 1998). Six years later, the extension of this catalog, ICRF-Ext.2, with 109 more sources, was published (Fey et al. 2004). However, the sky coverage of these catalogs was still not sufficient for some applications. Successful phase referencing requires a calibrator within 4° of the target source with a precise position and known source structure. The probability of finding a calibrator from the ICRF-Ext.2 catalog within 4° of any random target above -45° declination is about 50%. Also, the ICRF catalog does not provide source maps. In order to overcome these deficiencies, twelve 24 hour observing sessions with the VLBA, called VLBA Calibrator Surveys, were performed. Analysis of these observations produced the VCS1 (Beasley et al. 2002) and VCS2 (Fomalont et al. 2003) catalogs of 1611 new sources not listed in the ICRF catalog. Approximately 80% of these sources are suitable as phase-referencing calibrators and as target sources for space geodesy programs.

Combining all suitable calibrators from the ICRF-Ext.2, VCS1, and VCS2 catalogs, we get a list of 1986 sources. Over 89.5% of the sky north of -45° declination, we find at least one calibrator within a 4° radius disk in any given direction. In this paper, we present an extension of the VCS1 and VCS2 catalogs, called the VCS3 catalog, mainly concentrating on the other 10.5% of the sky where the source density is lowest. Since the observations, calibrations, astrometric solutions, and imaging are similar to those of VCS1, for details the reader is referred to Beasley et al. (2002). In § 2, we describe the strategy for selecting the 450 candidate sources, observed in three 24 hr sessions with the VLBA. In § 3, we briefly outline the observations and data analysis. We present the catalog in § 4 and summarize our results in § 5.

2. SOURCE SELECTION

Having unlimited resources, one could try to observe all sources stronger than some limiting flux. However, only sources with bright, compact components can be detected with VLBI and might be useful for phase referencing or geodetic applications. Kellermann et al. (1968) first showed that the distribution of sources over spectral index α ($F \propto \nu^\alpha$) has two peaks: one near $\alpha = -1$ (steep spectrum) and another near $\alpha = 0$

[1] Jansky Fellow, National Radio Astronomy Observatory.

(flat spectrum). Later it was confirmed that extended objects dominate in the steep-spectrum population (see the review by Kellermann & Owen 1988). In compact regions, which exhibit the synchrotron mechanism of emission, the peak in the spectrum caused by synchrotron self-absorption appears at frequencies higher than 1 GHz because of the regions' small size. Thus, if a dominating emission comes from compact regions, the spectrum of the total flux density will be predominantly flat or inverted.

Examining spectral indices in the PKSCAT90 catalog (Wright & Otrupcek 1990), which is believed to be complete at the 95% level for sources with flux density $F > 0.25$ Jy at 2.7 GHz (Bolton et al. 1979), we found that only 26% of sources have spectral indices $\alpha > -0.5$. Myers et al. (2003) used the NVSS (Condon et al. 1998) and GB6 (Gregory et al. 1996) catalogs to select sources with spectral indices above -0.5 at 5 GHz and found 11,685 sources brighter than 30 mJy, or 24% of the total number of sources. It should be noted that a significant fraction of the sources with spectral index in the range $[-0.5, -0.4]$ belong to the steep-spectrum population and are expected to have extended structure. Thus, taking sources at random the probability that a source will be compact and, therefore, detectable with VLBI does not exceed 20%. A carefully designed strategy for source selection can significantly increase the yield of detections.

We considered all bright sources at X band (8.6 GHz) and S band (2.3 GHz) with spectral indices greater than -0.5 as candidates for the VCS3 campaign. In order to find these sources, we first analyzed catalogs of compact flat-spectrum sources—JVAS (Wrobel et al. 1998), CLASS (Myers et al. 2003), the Parkes quarter-jansky catalog (Jackson et al. 2002), and the southern VLA catalog (Winn et al. 2003)—and selected all sources brighter than 100 mJy at declinations above -45° with arc distances from any known calibrator greater than $3\overset{\circ}{.}9$. This produced a list of 374 sources. Not all of these catalogs provide flux densities at more than one band. We used the CATS database (Verkhodanov et al. 1997) to cross-check the reported flux density and to acquire information about flux measurements for these objects from other sources. Unfortunately, most of these measurements were done at different epochs. Since many flat-spectrum sources are variable, the estimates of the spectral index made at different epochs may be unreliable. Instantaneous 1–22 GHz broadband spectra at four to six frequencies for 3000 active galactic nuclei with flux densities greater than 100 mJy at 2.3 GHz and $\alpha > -0.5$, including many sources from this list, were observed with the 600 m ring radio telescope RATAN-600 of the Russian Academy of Sciences in transit mode as a part of an ongoing survey program (see Kovalev et al. 1999 for the method of observation and data reduction). All flat-spectrum sources from this sample with flux densities greater than 200 mJy at X or S band and not previously observed with VLBI, a total of 116 sources, were included in the list of VCS3 candidates. After cross-checking we removed sources from the list for which the estimate of the spectral index was either unreliable or less than -0.5. The total number of sources selected from these catalogs was 300.

After picking up these 300 sources from all known compact flat-spectrum catalogs, we still had areas where the density of calibrators was less than the targeted density. In order to fill these areas, we used the NVSS catalog of about 1.8 million sources (Condon et al. 1998). First we selected 2704 sources with total flux density greater than 100 mJy at 1.4 GHz in the areas where the distance to the closest calibrator and already selected candidates was greater than 4°. The NVSS catalog does not provide information about spectral index, so we checked these 2704 sources against the CATS database, which nowadays contains one of the most complete collections of radio catalogs, and found the sources that had been observed under other campaigns at different frequency bands. If a source was not found in any other catalog, for example, was absent from the GB6 catalog, with flux limit 18 mJy, and the PMN catalog (Wright et al. 1996), with flux limit 40–70 mJy at 5 GHz, this indicates with high probability that the spectral index is significantly less than -0.5. In total, this initial list had 302 sources.

We examined the spectrum provided by CATS and subjectively ascribed a class to each source:

0. The source has a flat spectrum, the estimate of the spectral index is reliable (e.g., a RATAN-600 instantaneous spectrum is available), and the estimated correlated flux density is greater than 100 mJy.
1. The estimate of the spectral index is less reliable, or the spectral index is in the range $[-0.4, -0.2]$, and the estimated correlated flux density is greater than 100 mJy.
2. The estimate of the spectral index is unreliable or in the range $[-0.5, -0.4]$, or the estimated correlated flux density is less than 100 mJy.

Then, for each source we computed a score based on angular distance to the closest calibrator, flux density, spectral index, and class:

$$S = 10^3[(D - D_{\rm lim})/D_{\rm lim}]^3 + 10^5(\alpha + 0.5)^3 + 2 \times 10^2(2 - C) + \log F, \quad (1)$$

where D is the angular distance to the closest calibrator or already selected candidate, $D_{\rm lim}$ is the minimum angular distance (4°), α is the spectral index, C is the class, and F is the flux density in janskys, extrapolated to 8.6 GHz. An iterative procedure computed the score, selected the source with the largest score, and ran again. Using this method, we selected 150 sources with the highest scores in addition to the 300 sources previously chosen.

3. OBSERVATIONS AND DATA ANALYSIS

The VCS3 observations were carried out in three 24 hr observing sessions with the VLBA on 2004 April 30, May 8, and May 27. Since the correlated flux density for selected candidates was expected to be different, we split our sources into three categories:

(*a*) Sources of class 0 brighter than 200 mJy;
(*b*) Sources of class 0 with flux density in the range 100–200 mJy or sources of class 1 brighter than 200 mJy; and
(*c*) All other sources.

Integration times were chosen to be 90 s for sources from category *a*, 180 s from category *b*, and 300 s from category *c*. The sources above -20° declination were scheduled for two scans at different hour angles in order to improve the *u-v* coverage, while the sources in the $[-45^\circ, -20^\circ]$ declination range were scheduled for only one scan. The target sources were observed in a sequence designed to minimize loss of time from antenna slewing. In addition to the target sources, 77 strong sources were taken from the GSFC astrometric and geodetic catalog "2004a_astro."[2] Observations of three to four strong sources from this list were made every 1–1.5 hr during observing sessions. These observations were scheduled in such a way that

[2] See http://gemini.gsfc.nasa.gov/solutions/astro/.

at each station, at least one of these sources was observed at an elevation angle less than 20° and at least one at an elevation angle greater than 50°. The purpose of these observations was to provide calibration for mismodeled tropospheric path delays and to tie the VCS3 source positions to the ICRF catalog. On average, the antennas were on-source 70% of the time.

The observations used the VLBA dual-frequency geodetic mode, observing simultaneously at 2.3 and 8.6 GHz. Each band was separated into four intermediate-frequency channels, with bandwidth 8 MHz which spanned 140 MHz at 2.3 GHz and 490 MHz at 8.6 GHz, in order to provide precise measurements of group delays for astrometric processing. Since the a priori coordinates of many candidates were expected to have errors of up to 30″, the data were correlated with an accumulation period of 1 s in 64 frequency channels in order to provide extra-wide windows for fringe searching.

Processing of the VLBA correlator output to obtain the astrometric observables was performed using the Astronomical Image Processing System (AIPS; Greisen 1990). First, phases of the calibration signals injected into the receivers were subtracted from the fringe phases for each scan and each channel. Then the phases of a single strong calibrator scan were subtracted from each scan to flatten out the phases across the band of each individual channel. Sampler-bias correction, together with initial amplitude calibration, was performed using the recorded system temperatures and gain tables (tasks ACCOR and APCAL). The task FRING was then run for each baseline separately (with signal-to-noise cutoff of SNR = 3) to obtain the residual narrowband group delays for each channel, residual single-channel fringe phases, and residual single-channel phase delay rates. Task MBDLY was then used to compute the residual group delays from the four single-channel fringe phases at each frequency band. Then task CL2HF was used to compute the total group delays, phase delay rates, and fringe phases by combining the residuals with the correlator model and converting them from geocentric to reference-station quantities. Finally, the AIPS output was reformatted for input into the CALC/SOLVE geodetic-astrometric VLBI analysis software package[3] using task HF2SV.

CALC/SOLVE was used to determine accurate positions for all detected sources. Astrometric analysis was performed in several steps. First, we used narrowband group delays determined over each 8 MHz wide intermediate-frequency channel and incoherently averaged separately over all channels within the X and S bands. Narrowband group delays are less precise than wideband group delays but have very wide ambiguity spacings: 4 μs. In the first step, X-band single-band delay data (and S-band data for the sources detected only at S band) were used for estimation of new source positions, and clock functions were modeled by second-degree polynomials. These position estimates were used in an S-band wideband group-delay solution for short baselines between the stations at Pie Town, Kitt Peak, Owens Valley, Los Alamos, and Fort Davis in order to resolve the group-delay ambiguities with spacings of 100 ns and then again solve for source positions in the second step. In step 3, these estimates were used in an S-band group-delay solution for longer baselines for further ambiguity resolution. In the fourth step, the previous estimates of source positions were used for ambiguity resolution of X-band group delays (with spacings of 29 ns) on short baselines and a new solution was made. These estimates were then used to resolve X-band group delays at long baselines in the next step. In the sixth step, ionosphere-free combinations of X- and S-band wideband group delays were used for data analysis. The estimation model at this step included coefficients of linear splines for the clocks of all stations, except a reference station, and tropospheric zenith path delays at all sites. The time interval for linear splines was 60 minutes.

The data were carefully analyzed for the presence of any remaining errors in group-delay ambiguity resolution and for outliers. About 1% of the data were deselected, primarily because the fringe-fitting algorithm picked a secondary maximum of the delay resolution function. If only two observations of a source are used in a solution, errors in group-delay ambiguity resolution cannot be detected. However, if more observations are used in a solution, errors in group-delay ambiguity resolution can result in a significant misfit. Therefore, the analysis of observations of sources with numerous misfits allowed us to detect group-delay ambiguity resolution errors with at least three to six observations. Being conservative, we set a minimum number of eight observations needed to rule out the possibility of group-delay ambiguity resolution errors. After outlier elimination, we determined additive, baseline-dependent corrections to the a priori weights in such a manner that the ratios of the sums of weighted squares of postfit residuals to their mathematical expectation were close to unity.

In the final solution, all available astrometric and geodetic data from 1979 August to 2004 August, including the three VCS3 sessions, were used in a single least-squares solution. Estimated parameters included positions and velocities of stations, coordinates of all sources, Earth orientation parameters, clock functions, and tropospheric zenith path delays. The only differences in the treatment of the VCS3 sessions with respect to other experiments were that we did not estimate tropospheric gradients and the time intervals for clocks and tropospheric zenith path delays were 60 minutes instead of 20 minutes. Since a few sources were detected in only one band, we made three solutions: using (1) ionosphere-free linear combinations of X-band and S-band wideband group delays, (2) only X-band group delays, and (3) only S-band group delays.

Since the equation for time delay is invariant with respect to the group of coordinate transformations, observations themselves determine not source positions, but only a family of positions. In order to pick a specific member of this family, we imposed boundary conditions by applying net-rotation constraints on the positions of the 212 sources listed as "defining" in the ICRF catalog such that the set of new positions of these 212 sources did not have a net rotation with respect to the set of old positions from the ICRF. More details about this procedure can be found in Beasley et al. (2002).

In order to evaluate position errors, we made a special solution using only the three VCS3 sessions in which we estimated coordinates of all sources and applied no-net-rotation constraints on 20 sources common to the VCS3 and ICRF defining lists. Since 77 sources used in the VCS3 campaign were intensively observed earlier under various geodetic and astrometric programs, we used the differences between the very accurate positions derived from analysis of these observations and positions from the VCS3 sessions as a measure of the upper limit on VCS3 catalog errors. We represent estimates of the errors in right ascension (σ_α) and declination (σ_δ) of the VCS3 catalog in the form

$$\sigma_\alpha = \sqrt{(1.5\sigma_\alpha^r)^2 + [E_\alpha(\delta)/\cos\delta]^2},$$
$$\sigma_\delta = \sqrt{(1.5\sigma_\delta^r)^2 + E_\delta^2(\delta)}, \quad (2)$$

[3] See http://gemini.gsfc.nasa.gov/solve.

TABLE 1
Additive Corrections to Formal Uncertainties Applied for Derivation of Source Position Errors in the VCS3 Catalog

Declination Zone (deg)	X/S			X Band			S Band		
	Points	E_α (mas)	E_δ (mas)	Points	E_α (mas)	E_δ (mas)	Points	E_α (mas)	E_δ (mas)
(+20.0, +90.0).....	33	0.2	0.4	96	0.6	0.5	94	5.1	4.7
(0.0, +20.0).....	16	0.3	0.2	77	0.5	0.6	77	4.2	7.2
(−20.0, 0.0).....	11	0.2	0.3	64	0.8	1.5	64	7.0	16.8
(−30.0, −20.0).....	11	0.2	0.7	44	1.2	1.8	44	13.0	27.6
(−45.0, −30.0).....	13	0.3	0.4	76	2.4	7.3	75	40.0	40.0

where σ^r_α and σ^r_δ are the formal uncertainties derived from the error propagation law from fringe amplitude signal-to-noise ratios and E_α and E_δ are additive reweighting parameters. The multiplicative factor of 1.5 in equation (2), first found by Ryan et al. (1993), accounts for underestimated systematic errors in the computation of uncertainties of wideband group delays and affects the uncertainties in estimates of all parameters from VLBI, including source coordinates. We split the sources into five declination zones, and for each group we found the values of E_α and E_δ that made the ratio of the weighted sum of squares of residuals to their mathematical expectation close to unity. Using this technique, we computed additive corrections to the uncertainties in the estimates of X-band–only and S-band–only solutions by analyzing the differences between dual-band and single-band solutions. Reweighting parameters are presented in Table 1. A histogram of source position errors is presented in Figure 1.

For imaging purposes, the data were reprocessed with the global fringe-fitting procedure (task FRING) with an SNR cutoff of 4 at each individual channel. Global, station-based fringing allows detection of weaker sources than does the baseline-based fringing used for astrometric analysis. (We did not use global fringing for astrometric analysis, since, as we found earlier, it yields less reliable group delays than baseline-based fringing.) A bandpass correction was then determined with the task BPASS. After initial editing, the fringe amplitude and phases were averaged across the channels. We used the AIPS task CALIB in order to perform the first step of the self-calibration procedure applying the point-source model. The whole scan length was used to find the combined solution for the channels with an SNR cutoff of 3. After that, we imported data to the Caltech DIFMAP package (Shepherd 1997). We have adapted the automated procedure originally written by G. Taylor (see Pearson et al. 1994) for self-calibration and imaging of the VCS3 short snapshot observations.

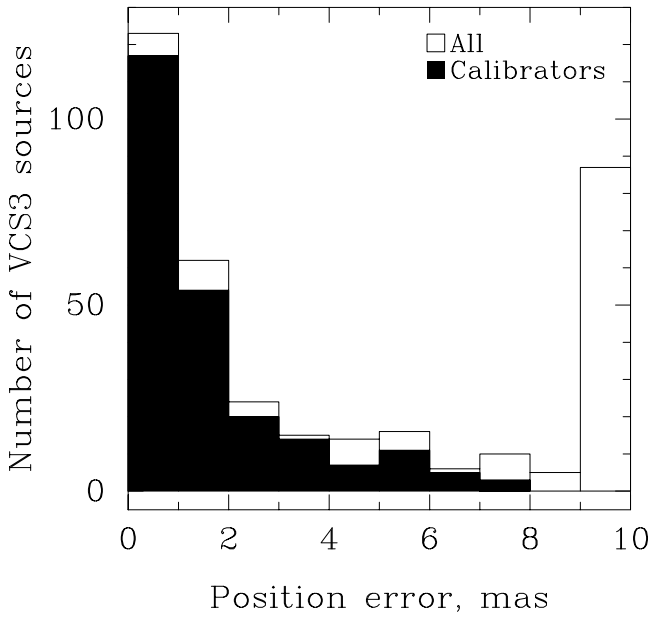

Fig. 1.—Histogram of semimajor error ellipse position errors. The rightmost bin shows all errors that exceed 9 mas.

For each detected source at each band, we computed two estimates of correlated flux density: one averaged over the entire image (total CLEAN flux density) and another averaged only over the spatial frequencies above 45 Mλ at S band and above 170 Mλ at X band, which correspond to the range [0.7, 1.0] of the maximum spatial frequency of the VLBA. The latter estimate characterizes the flux density of unresolved components. Errors in our estimates of the total correlated flux density of sources brighter than 100 mJy are determined mainly by the accuracy of amplitude calibration, which for the VLBA, according to Wrobel & Ulvestad (2004),[4] is at the level of 5% at 1–10 GHz. This estimate was confirmed by a comparison of the correlated flux density with the single-dish flux density measured with RATAN-600 in 2003 October for several slowly varying sources without extended structure. The contribution of fringe amplitude errors is significant for sources with flux density below 100 mJy. The error of correlated flux density for this group of sources is about 10%. It should be noted that in the case of a source with asymmetric extended structure, the estimate of the correlated flux density from unresolved components may be biased because of a significant nonuniformity of u-v coverage at long spacings.

In total, 365 out of 450 sources were detected and yielded at least two good points for position determination. However, not all of these sources are suitable as phase-referencing calibrators or as targets for geodetic observations. We consider a source suitable as a calibrator if (1) the number of good X-S pairs of observations is eight or greater, in order to rule out the possibility of a group-delay ambiguity resolution error, and (2) position error before reweighting is less than 5 mas. We found that eight observations at the VLBA are usually sufficient to obtain positions with errors of less than 5 mas. If the errors are significantly greater, this means that the source was not detected at long baselines, and therefore we do not possess information on whether the source can be detected when used as a phase-referencing calibrator. Only 231 sources satisfy these calibrator criteria. It should be mentioned that our criteria for the suitability of a source as a phase calibrator are rather conservative,

[4] Available at http://www.aoc.nrao.edu/vlba/obstatus/obssum/, section "Amplitude Calibration."

TABLE 2
THE VCS3 CATALOG

	Source Name		J2000.0 Coordinates		Errors (mas)				Correlated Flux Density (Jy)				
									8.6 GHz		2.3 GHz		
Class (1)	IVS (2)	IAU (3)	α (4)	δ (5)	$\Delta\alpha$ (6)	$\Delta\delta$ (7)	Correl. (8)	Obs. (9)	Total (10)	Unres. (11)	Total (12)	Unres. (13)	Band (14)
C	0001−120	J0004−1148	00 04 04.914997	−11 48 58.38564	0.24	0.40	−0.069	20	0.62	...	0.76	...	X/S
—	0003+340	J0006+3422	00 06 07.382435	+34 22 20.41138	1.83	4.46	−0.233	5	0.06	...	...	...	X
C	0009+655	J0012+6551	00 12 37.671095	+65 51 10.82363	9.21	4.00	0.040	10	0.12	...	0.69	...	X/S
—	0017+296	J0019+2956	00 19 37.791440	+29 56 01.93471	19.34	7.63	−0.015	14	...	...	0.08	...	S
—	0021−084	J0024−0811	00 24 00.672746	−08 11 10.05397	4.75	8.88	−0.124	7	0.08	0.06	0.09	0.06	X/S
C	0026−015	J0029−0113	00 29 00.986049	−01 13 41.76047	0.74	0.95	0.349	36	0.20	0.06	0.19	0.10	X/S
C	0027−024	J0030−0211	00 30 31.823755	−02 11 56.13361	0.30	0.57	−0.243	68	0.25	0.22	0.18	0.16	X/S
C	0029−147	J0031−1426	00 31 56.411853	−14 26 19.34670	0.93	1.60	−0.607	36	0.17	<0.06	0.23	0.13	X/S
C	0042+186	J0044+1855	00 44 42.227898	+18 55 05.03460	0.76	1.69	0.591	36	0.09	...	0.14	0.11	X/S
—	0042−373	J0045−3705	00 45 12.065955	−37 05 48.47087	3.05	7.43	−0.066	20	0.20	0.19	...	...	X
C	0043+246	J0046+2456	00 46 07.825737	+24 56 32.52438	0.26	0.46	0.051	90	0.44	0.33	0.18	0.15	X/S
C	0046+063	J0048+0640	00 48 58.723150	+06 40 06.47544	0.67	1.20	0.414	28	0.13	0.06	0.24	0.06	X/S
C	0054+161	J0056+1625	00 56 55.294324	+16 25 13.34088	0.33	0.29	0.019	90	0.42	0.40	0.27	0.26	X/S
C	0055+060	J0058+0620	00 58 33.804481	+06 20 06.07358	0.68	1.31	−0.221	19	0.17	0.15	0.09	<0.06	X/S

NOTE.—Table 2 is presented in its entirety in the electronic edition of the Astronomical Journal. A portion is shown here for guidance regarding its form and contents. Units of right ascension are hours, minutes, and seconds, and units of declination are degrees, arcminutes, and arcseconds.

and sources that fail these criteria may still be useful for some applications.

Five detected sources turned out to be known gravitational lenses. Since the fringe amplitude may have several minima and maxima during the integration time for such a source, our technique for fringe searching is not applicable. We excluded these gravitational lenses from the analysis, since they are certainly not suitable as calibrators.

4. THE VCS3 CATALOG

The VCS3 catalog is presented in Table 2. The first column gives source class: "C" if the source can be used as a calibrator, and a dash if it cannot. The second and third columns give the IVS name (B1950 notation) and the IAU name (J2000 notation). The fourth and fifth columns give source coordinates at the J2000.0 epoch. Columns (6) and (7) give inflated source position uncertainties in right ascension and declination in milliarcseconds, and column (8) gives the correlation coefficient between the errors in right ascension and declination. The number of group delays used for position determination is listed in column (9). The next two columns give the estimates of correlated flux density in janskys at X band: total CLEAN flux density (col. [10]) and flux density of unresolved components (col. [11]). Similar information for S band is listed in columns (12) and (13). For some sources, only estimates of the total VLBA flux density are presented, because either no data at long baselines were collected or the data at these baselines were unreliable. Column (14) gives the data type used for position estimation: "X/S" stands for an ionosphere-free linear combination of X and S wideband group delays, "X" stands for X-band–only group delays, and "S" stands for S-band–only group delays. Some sources that yielded fewer than eight pairs of X- and S-band group-delay observables had two or more observations at X and/or S band observations. For these sources, either X-band–only or S-band–only estimates of coordinates are listed in the VCS3 catalog, whichever uncertainty is less.

In addition to this table, an HTML version of the catalog is available on the World Wide Web.[5] For each source, it has eight links: to a pair of PostScript maps of the source at X and S bands, to a pair of plots of correlated flux density as a function of the length of the baseline projection to the source plane, to a pair of FITS files with naturally weighted CLEAN images, and to a pair of FITS files with calibrated *u-v* data. The coordinates and the plots are also accessible from the NRAO VLBA Calibration Search Web page.[6]

A sample of the data used for candidate selection, as well as some typical imaging results, is shown in Figure 2. In Figure 2*a*, we present the broadband spectra from RATAN-600 observations in 2003 and from some old data taken from the NVSS, the 87GB (Gregory & Condon 1991), and the Fürst et al. (1990) 11 cm radio survey of the Galactic plane catalogs. In Figures 2*b* and 2*d* the dependence of visibility function amplitude versus projected baseline at S and X bands, respectively, is shown. Each point is a coherent average over the scan duration and over the band. Naturally weighted CLEAN images at S and X bands are presented in Figures 2*c* and 2*e*.[7] The sources in this figure are placed such that the contribution of the compact component to the total emission increases from left to right. According to Kovalev et al. (2002), we interpret the broadband spectra of all selected sources as a sum of two constituents: emission from an optically thin, extended component with a steep spectrum that usually increases with decreasing frequency up to hundreds of megahertz, and emission from a compact component with self-absorption that has a maximum at a frequency higher than 1 GHz. The spectrum of J0012+6551 has spectral index −0.5. No contribution to emission from the compact component is seen, and the correlated flux density even at the shortest-baseline projections is several times less than the total flux density (see the discussion of angular dimensions of

[5] At http://gemini.gsfc.nasa.gov/vcs3/.
[6] See http://magnolia.nrao.edu/vlba_calib/.
[7] The scale of the J0012+6551 map has been increased with respect to the other maps.

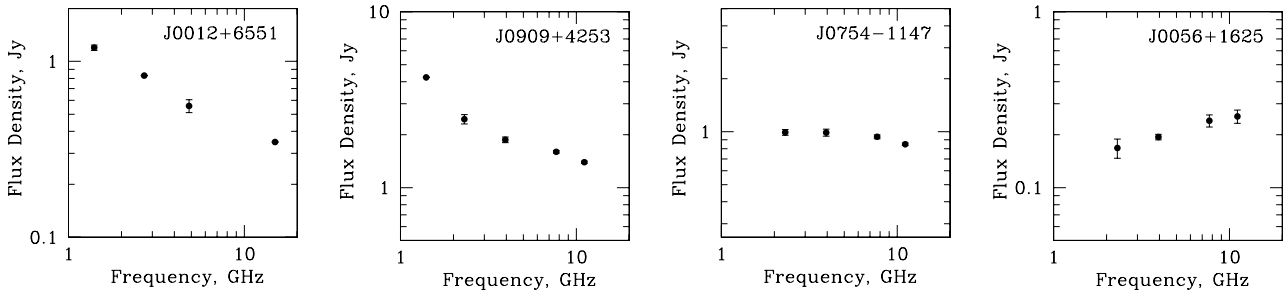

FIG. 2*a*

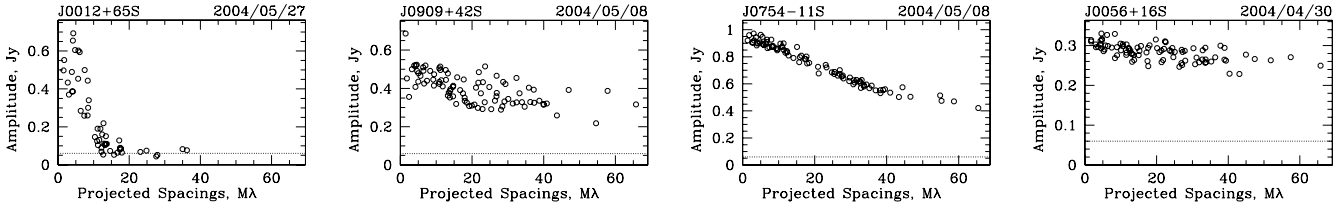

FIG. 2*b*

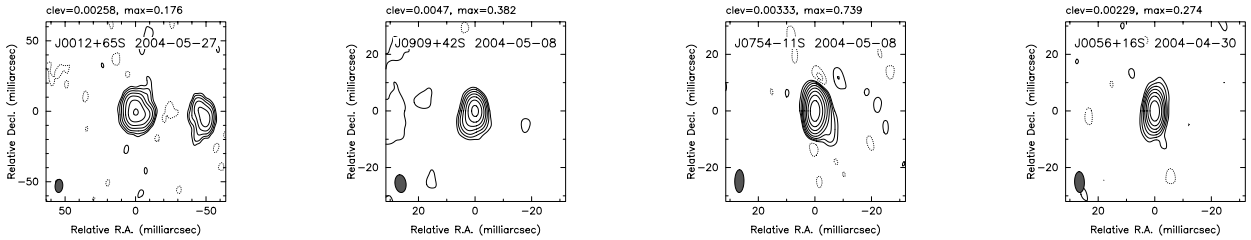

FIG. 2*c*

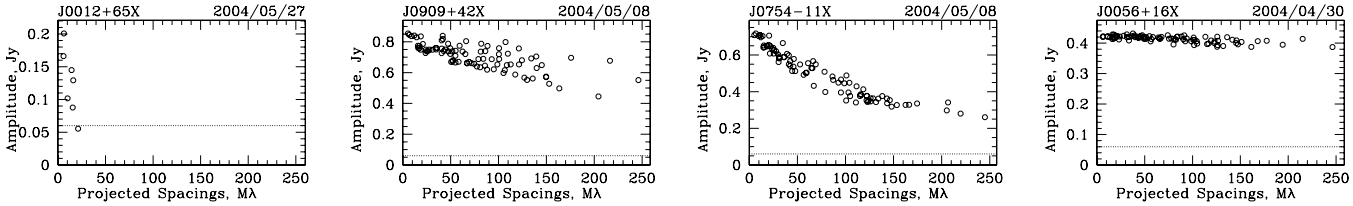

FIG. 2*d*

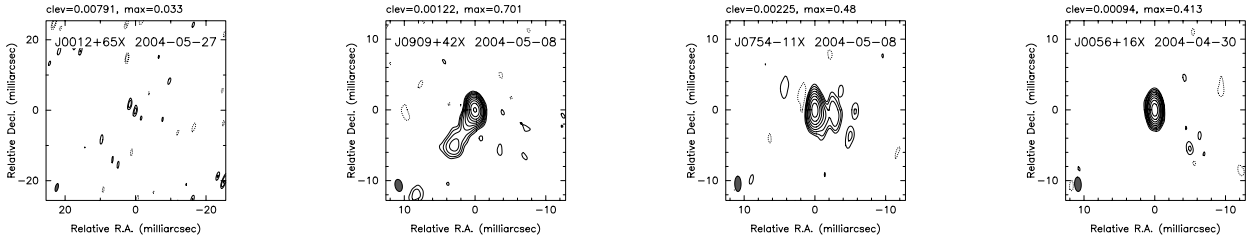

FIG. 2*e*

FIG. 2.—(*a*) Broadband spectra from RATAN-600 observations in 2003 plus data from CATS. (*b*) Dependence of the correlated flux density at S band (2.3 GHz) on projected spacing. Dotted lines show the detection limit. (*c*) Naturally weighted CLEAN images at S band. The lowest contour levels (two steps) are plotted at "clev" (=3 times rms noise) levels (Jy beam^{-1}), and the peak brightness at "max" values (Jy beam^{-1}). Dotted contours indicate negative flux. The beam is shown in the lower left corner of the images. (*d*) Dependence of the correlated flux density at X band (8.6 GHz) on projected spacing. (*e*) Naturally weighted CLEAN images at X band.

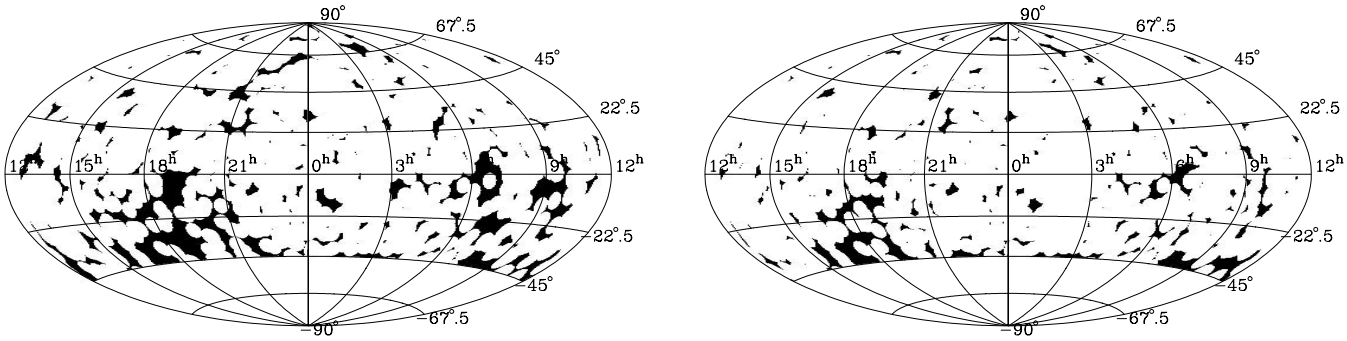

FIG. 3.—Source sky density before (*left*) and after (*right*) the VCS3 observing campaign. The area above −45° declination with calibrator source density less than one source within a 4° radius disk is shown in black.

compact steep-spectrum sources by O'Dea [1998] for more details). The source is below the detection limit at both bands at spacings longer than 20 Mλ. At X band the map shows only noise. The spectrum of J0909+4253 has a spectral index of −1.1 at frequencies less than 2 GHz, and it flattens at higher frequencies. This flattening is caused by the contribution of the compact component. When the contribution of the extended component is subtracted from the spectrum, the residual spectrum grows with increasing frequency, and our measurements of the correlated flux density confirm this. The remaining two sources have flat and inverted spectra, which is an indication of the dominance of the compact constituent in the total emission. Again, our VLBA observations confirm this. Correlated flux densities at short spacings for J0056+1625 and some other sources are even higher than the total flux density observed at RATAN half a year before the VLBA measurements, because of the strong variability of the object. Analysis of this sample illustrates the validity of our approach for candidate selection.

5. CONCLUSION

The VCS3 has added 360 new sources not previously observed with VLBI. Of these, 231 sources are suitable as phase-referencing calibrators and as target sources for geodetic applications. A careful strategy of source selection resulted in a very high detection rate; more than 80% of the sources in our candidates list were detected.

This campaign has contributed considerably to reducing the areas of sky with a low density of known calibrators. If only sources from the ICRF-Ext.2 are taken into account, 48.1% of the sky area above declination −45° has no calibrator within a 4° radius disk in any given direction. Combining the ICRF-Ext.2 and the VCS1 catalogs, this area is reduced to 13.7%. Adding the VCS2 catalog reduces the area to 10.5%. After the VCS3 campaign, this area is only 5.3% of the sky above declination −45°. Figure 3 shows the area with insufficient calibrator density before and after the VCS3 observing campaign.

The National Radio Astronomy Observatory is a facility of the National Science Foundation operated under cooperative agreement by Associated Universities, Inc. The authors made use of the CATS database of the Special Astrophysical Observatory of the Russian Academy of Sciences. This research has made use of the NASA/IPAC Extragalactic Database, which is operated by the Jet Propulsion Laboratory, California Institute of Technology, under contract with the National Aeronautics and Space Administration. RATAN-600 observations were partly supported by the Russian State Program "Astronomy" and the Russian Ministry of Education and Science, the NASA JURRISS program (project W-19611), and the Russian Foundation for Basic Research (projects 01-02-16812 and 02-02-16305). The authors are grateful to D. MacMillan for valuable comments. This work was performed while L. P. and D. G. worked for NVI, Inc., and Raytheon, respectively, under NASA contract NAS 5-01127.

REFERENCES

Beasley, A. J., Gordon, D., Peck, A. B., Petrov, L., MacMillan, D. S., Fomalont, E. B., & Ma, C. 2002, ApJS, 141, 13
Bolton, J. G., Savage, A., & Wright, A. E. 1979, Australian J. Phys. Astrophys. Suppl., No. 46, 1
Cohen, M. H., & Shaffer, D. B. 1971, AJ, 76, 91
Condon, J. J., Cotton, W. D., Greisen, E. W., Yin, Q.-F., Perley, R. A., Taylor, G. B., & Broderick, J. J. 1998, AJ, 115, 1693
Fey, A. L., et al. 2004, AJ, 127, 3587
Fomalont, E., Petrov, L., MacMillan, D. S., Gordon, D., & Ma, C. 2003, AJ, 126, 2562
Fürst, E., Reich, W., Reich, P., & Reif, K. 1990, A&AS, 85, 805
Gregory, P. C., & Condon, J. J. 1991, ApJS, 75, 1011
Gregory, P. C., Scott, W. K., Douglas, K., & Condon, J. J. 1996, ApJS, 103, 427
Greisen, E. W. 1990, in Acquisition, Processing and Archiving of Astronomical Images, ed. G. Longo & G. Sedmak (Naples: Oss. Astron. Capodimonte), 125
Jackson, C. A., Wall, J. V., Shaver, P. A., Kellermann, K. I., Hook, I. M., & Hawkins, M. R. S. 2002, A&A, 386, 97
Kellermann, K. I., & Owen, F. N. 1988, in Galactic and Extragalactic Radio Astronomy, ed. G. L. Verschuur & K. I. Kellermann (2nd ed.; Berlin: Springer), 563
Kellermann, K. I., Pauliny-Toth, I. I. K., & Davis, M. M. 1968, Astrophys. Lett., 2, 105
Kovalev, Y. Y., Kovalev, Yu. A., Nizhelsky, N. A., & Bogdantsov, A. B. 2002, Publ. Astron. Soc. Australia, 19, 83
Kovalev, Y. Y., Nizhelsky, N. A., Kovalev, Yu. A., Berlin, A. B., Zhekanis, G. V., Mingaliev, M. G., & Bogdantsov, A. V. 1999, A&AS, 139, 545
Ma, C., et al. 1998, AJ, 116, 516
Matveenko, L. I., Kardashev, N. S., & Sholomitskii, G. B. 1965, Radiofizika, 8, 651 (English transl. Soviet Radiophys., 8, 461)
Myers, S. T., et al. 2003, MNRAS, 341, 1
O'Dea, C. P. 1998, PASP, 110, 493
Pearson, T. J., Shepherd, M. C., Taylor, G. B., & Myers, S. T. 1994, BAAS, 26, 1318
Ryan, J. W., Clark, T. A., Ma, C., Gordon, D., Caprette, D. S., & Himwich, W. E. 1993, in Contributions of Space Geodesy to Geodynamics: Crustal Dynamics, ed. D. E. Smith & D. L. Turcotte (Washington: Am. Geophys. Union), 37

Shepherd, M. C. 1997, in ASP Conf. Ser. 125, Astronomical Data Analysis Software and Systems VI, ed. G. Hunt & H. E. Payne (San Francisco: ASP), 77
Verkhodanov, O. V., Trushkin, S. A., Andernach, H., & Chernenkov, V. N. 1997, in ASP Conf. Ser. 125, Astronomical Data Analysis Software and Systems VI, ed. G. Hunt & H. E. Payne (San Francisco: ASP), 322
Winn, J. N., Patnaik, A. R., & Wrobel, J. M. 2003, ApJS, 145, 83
Wright, A. E., Griffith, M. R., Hunt, A. J., Troup, E., Burke, B. F., & Ekers, R. D. 1996, ApJS, 103, 145
Wright, A. E., & Otrupcek, R. 1990, PKSCAT90 Radio Source Catalogue and Sky Atlas (Epping: Australia Telesc. Natl. Facility)
Wrobel, J. M., Patnaik, A. R., Browne, I. W. A., & Wilkinson, P. N. 1998, BAAS, 30, 1308
Wrobel, J. M., & Ulvestad, J. S. 2004, Very Long Baseline Array Observational Status Summary (Socorro: NRAO)